Title
APPROXIMATE DIFFERENTIAL CROSS SECTIONS AT LARGE SCATTERING ANGLES FOR SIMPLE REPULSIVE POTENTIALS

Author
Gislason, E.A.

Publication Date
1971-06-01

Submitted to Journal of
Chemical Physics

UCRL-20712
Preprint

APPROXIMATE DIFFERENTIAL CROSS SECTIONS AT LARGE SCATTERING ANGLES FOR SIMPLE REPULSIVE POTENTIALS

E. A. Gislason

June 1971

AEC Contract No. W-7405-eng-48

LAWRENCE RADIATION LABORATORY
UNIVERSITY of CALIFORNIA BERKELEY

UCRL-20712

DISCLAIMER

Approximate Differential Cross Sections at Large Scattering Angles for Simple Repulsive Potentials.

E. A. Gislason*

Department of Chemistry and Inorganic Materials Research Division of the Lawrence Radiation Laboratory, Berkeley, California

ABSTRACT

The classical deflection angle θ and the classical differential cross section $I(\theta)$ are examined in the region near $\theta = 180°$ for three simple repulsive potentials: the repulsive power potential; the exponential repulsive potential; and the screened Coulomb potential. An expansion for θ valid at small impact parameters is carried through second order and compared with exact calculations of θ and $I(\theta)$. In most cases, the expansion is quite accurate in the region from $\theta = 180°$ to $\theta = 80°$. Numerical formulas are given for evaluating the first two coefficients in the expansion. Interpretation of experimental cross sections using these results is discussed.

*Present address: Department of Chemistry, University of Illinois at Chicago Circle, Chicago, Illinois.

The calculation of classical deflection angles and differential cross sections for any reasonable potential is quite straightforward using modern computers. This problem has recently been discussed in great detail by Ioup and Thomas.[1] Exact values of differential cross sections for a number of simple potentials have appeared in the literature. As in most numerical calculations, however, it is only possible to list results for selected values of angle and relative energy. Thus, later workers must often repeat the same calculations when faced with different angles or energies.

Because of this problem, a number of approximations have been developed for special regions of angle and energy. A series expansion valid at large impact parameters (small scattering angles) was developed by Lehmann and Leibfried[2] and by Smith et al.[3] This series converges rapidly at high energy and has proved extremely useful in interpreting experiments at small angles including the "rainbow" angle region.[4] In this paper we will consider an analogous expansion for small impact parameter collisions. Recently a number of experiments have studied scattering in this region of large deflection angles.

Three simple repulsive potentials will be used as examples with this large-angle expansion. They are the repulsive power potential

$$V = K/r^s, \tag{1}$$

the exponential repulsive potential

$$V = A \exp(-r/a), \tag{2}$$

and the screened Coulomb potential

$$X = A(\tfrac{a}{R})\exp(-r/a). \tag{3}$$

For the first potential Felder[5] has given exact values of the deflection angle and cross secion for selected values of s. Everhart et al[6] have computed a few differential cross sections for the screened Coulomb potential, and Robinson[7] has compiled a large table of deflection angles for both the screened Coulomb and exponential repulsive potentials.

In this work we will closely examine the large-angle expansion. The first two terms of the expansion will be evaluated and compared with exact calculations. Both deflection angles and differential cross sections are considered. The region of convergence of the series is investigated, and useful numerical formulas for reproducing the first two terms of the series are presented.

THEORY

The classical deflection angle in the center of mass coordinate system is obtained from

$$\theta = \pi - 2b\int_{r_m}^{\infty} dr\ r^{-2}\ f(r)^{-\frac{1}{2}}, \tag{4}$$

where

$$f = 1 - V(r)/E - b^2/r^2, \tag{5}$$

b is the classical impact parameter, and $E = 1/2\,\mu v^2$ is the relative kinetic energy of the collision. The turning point, r_m, is the largest solution of the equation

$$f(r_m) = 0.$$

The classical differential cross section $I(\theta)$ can then be obtained from

$$I(\theta) = (b/\sin\theta)\left|\frac{d\theta}{db}\right|^{-1}. \tag{6}$$

Exact deflection angles have been evaluated for all three repulsive potentials using Eq. (4). The singularity at $r=r_m$ was removed using the transformation due to Burnett.[8] If we let

$$\begin{aligned} \alpha &= (1-z^2)\alpha_o \\ \sin\alpha &= b/r \\ \sin\alpha_o &= b/r_m, \end{aligned} \tag{7}$$

then

$$\theta = \pi - 4\alpha_o \int_o^1 dz\ z[1-V(b/\sin\alpha)/(E\cos^2\alpha)]^{-\frac{1}{2}}. \tag{8}$$

This integrand is well-behaved in the region 0 to 1, although it must be evaluated analytically at z = 0. The integral itself was done using Romberg quadrature to prescribed accuracy, usually 3 parts in 10^6. This accuracy was achieved in about 0.05 sec on a CDC 6600 computer. For the differential cross section the derivative $d\theta/db$ can be obtained using the equations in Ref. 1. Because we were not interested in extremely accurate values of $I(\theta)$, a simple three-point numerical differentiation of θ was used most of the time. Then $I(\theta)$ was accurate to 2 parts in 10^4, or better.

Approximate deflection angles are obtained by expanding Eq. (4) in an appropriate manner. For example, the expansion of Leibfried[2] and Smith[3] valid at large impact parameters is obtained by recognizing that V(r) is always small. Then Eq. (4) becomes

$$\theta = \sum_{n=0}^{\infty} E^{-(n+1)}\ \tau_n(b). \tag{9}$$

For the simple potentials discussed in this paper the first few values of $\tau_n(b)$ have been tabulated in Refs. 2 and 3. The expression we wish to study in detail is obtained by expanding the integrand in Eq. (4) for small impact parameter:

$$\theta = \pi - \sum_{n=0}^{\infty} \phi_n(E) b^{2n+1}. \tag{10}$$

The coefficients, as shown by Leibfried,[9] are computed from

$$\phi_n(E) = 2(n!)^{-1}(-1)^n \int_{r_o}^{\infty} dr (v)^{\frac{1}{2}} (1-v)^{-\frac{1}{2}} g_n(r) \tag{11}$$

with

$$g_n(r) = \frac{d^n}{dr^n}[(v^2/v')^n r^{-2(n+1)} v^{-(n+\frac{1}{2})}]. \tag{12}$$

Here $v = V(r)/E$, $v' = dv/dr$, and r_o is the turning point for collisions with $b = 0$. Thus,

$$v(r_o) = 1 \tag{13}$$

must be solved to find r_o.

Once the coefficients ϕ_n are computed, the differential cross section $I(\theta)$ can be computed from Eq. (6). This involves a series reversion which is easily carried out for the first few terms. For example, keeping terms through order ϕ_1, we get near $\theta=\pi$ the results

$$\pi - \theta = \phi_o b + \phi_1 b^3 + \ldots \tag{14}$$

$$I(\theta) = (\phi_o^2 \sin\theta)^{-1} (\pi-\theta)[1-(4\phi_1/\phi_o^3)(\pi-\theta)^2 + \ldots]. \tag{15}$$

The last equation shows the well known result that $I(\theta=\pi) = \phi_o^{-2}$. Although the term $\sin\theta$ can be expanded in a power series in $(\pi-\theta)$, it is best to leave Eq. (15) as written. This is because Eq. (14) with just two terms is often accurate out to $\theta = \pi/2$, whereas similar accuracy in $\sin\theta$ would require at least four terms.

Unfortunately, the infinite series in Eqs. (9) and (10) both diverge, typically between $\theta=90°$ and $\theta=20°$. Leibfried[10] has examined this problem in detail. He examined successive terms in the series in the limit of large n and determined at what impact parameter b (for a given E) each series diverges. There is, in general, a region where neither series converges. Because we hope to use these series

in conjuction with experiments, which determine θ rather than b, we will be interested in recasting his results concerning series divergence in terms of angles.

We will use the results of this section to consider the three potentials individually. The values of ϕ_0 and ϕ_1 for all energies of interest are determined, and simple polynomial approximations are given for them. The approximate differential cross section computed from Eq. (15) is then compared with the exact result. It is shown that for most energies Eq. (15) works surprisingly well out to $\theta = \pi/2$ and even beyond.

REPULSIVE POWER POTENTIAL

The coefficients for the repulsive power potential in Eq. (1) have been evaluated analytically by Leibfried,[9] who obtained

$$\phi_n(E) = (2/s)(E/K)^c(n+1/2-c)^{-1}\, B(1/2,c)/B(n+1,1/2-c), \qquad (16)$$

where

$$c = (2n+1)/s, \qquad (17)$$

and B (x,y) is the Beta function, defined in terms of the Gamma function as

$$B(x,y) = \Gamma(x)\Gamma(y)/\Gamma(x+y). \qquad (18)$$

In particular, we have

$$\phi_0(E) = (E/K)^{1/s}\ (2/s)\Gamma(1/2)\Gamma(1/s)/\Gamma(1/2+1/s) \qquad (19)$$

$$\phi_1(E) = (E/K)^{3/s}\ s^{-2}(s-6)\Gamma(3/s)\Gamma(1/2)/\Gamma(1/2+3/s). \qquad (20)$$

Since the quantity $(K/E)^{1/s}$ has units of length, the reduced differential cross section at $\theta=\pi$ is

$$I(\pi)/(K/E)^{2/s} = i(s) \qquad (21)$$

with

$$i(s) = (s^2/4)\Gamma(1/2+1/s)^2/[\Gamma(1/2)\Gamma(1/s)]^2. \qquad (22)$$

A plot of i(s) is shown in Fig. (1). Assuming s is known, an absolute measurement of $I(\pi)$ will yield the constant K. Any experimental uncertainty in $I(\pi)$ or s, however, will lead to uncertainties in V(r). For example, if s=8 a 4% error in $I(\pi)$ gives a 17% error in K. An uncertainty in s has a more complicated effect on the potential. To show this in detail we have worked out an example. Assume an experiment at 1 eV measures $I(\pi) = 0.1\text{Å}^2/\text{sr}$. If the true potential has s=8, Eq. (21) gives the potential drawn in Fig. (2). The same data interpreted with other values of s gives rather different potentials, also shown in Fig. (2). Thus, the closer s is to the true value, the better the potential, but it is hard to generalize beyond this.

The potential parameter s can be obtained from the behavior of $I(\theta)$ away from $\theta=\pi$. We can rewrite Eq. (15) as

$$\sin\theta\,(\pi-\theta)^{-1}I(\theta)/I(\pi) = 1-h(s)(\pi-\theta)^2 + \ldots \qquad (23)$$

with

$$h(s) = (2\pi)^{-1}(s)(s-6)[\Gamma(1/2+1/s)/\Gamma(1/s)]^3\Gamma(3/s)/\Gamma(1/2+3/s). \qquad (24)$$

The function h(s) is shown in Fig. (1). It varies from 1/6 (the hard sphere result) at large s to $-\sqrt{3}/\pi$ at s=0, passing through zero at s=6. This means that the right hand side of Eq. (23) is slowly varying near $\theta=\pi$; even at $\theta=\pi/2$ the first two terms can only be as large as 2.36 or as small as 0.59. The implication for experimental work is clear. Measurements of $I(\theta)/I(\pi)$ at large deflection angles will give a good value for s only if the measurements are quite accurate. For example, near s=8 a 1% error in $I(\theta)$ at $\theta=\pi/2$ would

give a 3.4% error in s. This problem is not as severe if the measurements are extended to smaller angles, but then Eq. (23) may no longer converge and exact calculations of $I(\theta)$ would be necessary.

We have compared the exact differential cross section $I(\theta)$ with the two-term approximation in Eq. (23). Figure (3) shows the angle (for each s) where the exact and approximate cross sections differ by 5%; for all angles larger than this Eq. (23) can be used quite confidently. For comparison, Fig. (3) also gives the angle at which the series in Eq. (10) no longer converges; this involves converting Leibfried's[10] results from impact parameters to angles. Thus the first curve shows the angular region where two terms of Eq. (23) gives $I(\theta)$ accurately; the second curve shows the region where an infinite number of terms would give $I(\theta)$ accurately.

EXPONENTIAL REPULSIVE POTENTIAL

The coefficients ϕ_n for the exponential repulsive potential $V=A\exp(-r/a)$ must be evaluated numerically from Eq. (11).

The first two coefficients can be written.

$$\phi_o = (2/a)\int_o^\infty dx\ (x+R_o)^{-2}(1-e^{-x})^{-\frac{1}{2}} \qquad (25)$$

$$\phi_1 = a^{-3}\int_o^\infty dx\ (x+R_o-8)(x+R_o)^{-5}(1-e^{-x})^{-\frac{1}{2}}. \qquad (26)$$

Here we have set $R_o = r_o/a$, and using Eq. (13) we can easily show that

$$R_o = \ln(A/E). \qquad (27)$$

Although these integrals can not be done analytically, they can be expanded for the cases of small R_o and large R_o.

For <u>small</u> R_o, the expression $(1-e^{-x})^{-\frac{1}{2}}$ is expanded for small x, and the resulting integrals are Beta functions. The series terminates

when the appropriate integral does not converge at $x=\infty$. The results are:

$$a\phi_o = \pi R_o^{-3/2}[1+1/4R_o] \tag{28}$$

$$a^3\phi_1 = -(35\pi/16)R_o^{-9/2} \sum_{n=o}^{4} C_n R_o^n \tag{29}$$

The coefficients C_n are tabulated in Table I.

For <u>large</u> R_o the expansion is worth examining in some detail. For all x we can write

$$(1-e^{-x})^{-1/2} = \sum_{k=o}^{\infty} A_k e^{-kx} \tag{30}$$

with

$$A_k = \Gamma(2k+1)/[2^k\Gamma(k+1)]^2. \tag{31}$$

Using this and the substitution $y=(x+R_o)/R_o$, Eq. (25) becomes

$$\begin{aligned} a\phi_o &= (2/R_o)\sum_{k=o}^{\infty} A_k e^{kR_o}\int_1^{\infty} dy e^{-kR_o y}\, y^{-2} \\ &= (2/R_o) + (2/R_o)\sum_{k=1}^{\infty} A_k e^{kR_o} E_2(kR_o). \end{aligned} \tag{32}$$

The function $E_2(X)$ is the exponential integral,[11] whose asymptotic expansion for large x is well known:

$$E_2(x)\sim(e^{-x}/x)[1-(2/x)+(6/x^2)-(24/x^3)+(120/x^4)- \ . \ . \ .].$$

Combining this with Eq. (32) gives

$$\begin{aligned} a\phi_o = (2/R_o)+(2S_1/R_o^2)-(4S_2/R_o^3)+(12S_3/R_o^4) \\ -(48S_4/R_o^5)+(240S_5/R_o^6)- \ . \ . \ . \ , \end{aligned} \tag{33}$$

where the sums S_n are given by

$$S_n = \sum_{k=1}^{\infty} A_k/k^n \ . \tag{34}$$

Since $A_k \sim k^{-1/2}$ for large k, S_n converges for $n>1/2$ and very rapidly for large n. Conveniently, A_1, which converges very slowly, can be evaluated analytically. Using Eq. (30), we know that

$$x^{-1}(1-x)^{-1/2} - x^{-1} = \sum_{k=1}^{\infty} A_k x^{k-1}$$

Integrating both sides from 0 to 1 gives

$$S_1 = \sum_{k=1}^{\infty} A_k/k = \ln 4. \tag{35}$$

For n=2 and higher, the values of S_n were obtained by directly summing Eq. (34), using double precision on an IBM 360/65. Eight place accuracy required 2×10^6 terms for S_2 or about 3 minutes of computer time. The values of S_1 through S_5 are given in Table II.

With these numbers the expansions for ϕ_o and ϕ_1 at large R_o can be summarized as follows:

$$a\phi_o = (2/R_o) \sum_{n=o}^{\infty} G_n R_o^{-n} \tag{36}$$

$$a^3\phi_1 = (3R_o^3)^{-1} \sum_{n=o}^{\infty} H_n R_o^{-n} \tag{37}$$

The first five coefficients G_n and H_n are tabulated in Table I.

Unfortunately, there is a region of R_o where neither expansion gives accurate values for ϕ_o and ϕ_1. Thus, it is necessary to integrate Eqs. (25) and (26) numerically. We have done this for many values of R_o and then fit the coefficients by least squares to polynomials in R_o. These <u>numerical</u> approximations for ϕ_o and ϕ_1 have been determined for all values of R_o greater than zero. The results are summarized below:

<u>$0 < R_o \leq 0.1$</u>

$$a\phi_o = 3.1416R_o^{-3/2}(1+0.2500R_o-0.134R_o^2) \tag{38}$$

$a^3\phi_1$ (use Eq. (40) below)

<u>$0.1 \leq R_o \leq 2.4$</u>

$$a\phi_o = 3.1432R_o^{-3/2} \sum_{n=o}^{5} D_n R_o^n \tag{39}$$

$$a^3\phi_1 = -6.8721R_o^{-9/2} \sum_{n=o}^{} E_n R_o^n \tag{40}$$

<u>$2.4 \leq R_o \leq 6.9$</u>

$$a\phi_o = 4.6200R_o^{-1} \sum_{n=o}^{5} I_n R_o^n \tag{41}$$

$$a^3\phi_1 = -3.5738R_o^{-5} \sum_{n=o}^{5} J_n R_o^n \tag{42}$$

$6.9 \leq R_o \leq 16.1$

$$a\phi_o = 2.0027\ R_o^{-1} \sum_{n=o}^{2} K_n R_o^{-n} \tag{43}$$

$$a^3\phi_1 = 0.33427\ R_o^{-3} \sum_{n=o}^{4} L_n R_o^{-n} \tag{44}$$

The coefficients D_n, E_n, I_n, J_n, K_n, and L_n are given in Table III. For R_o greater than 16.1, Eqs. (36) and (37) can be used. The accuracy of every series above but one is better than 1 part in 10^4 for all R_o. The coefficient ϕ_1 goes through zero near $R_o = 6.6$; thus, in the vicinity numbers computed from Eq. (42) may have an absolute error of 2×10^{-8} or a fractional error of 1×10^{-4}, whichever is greater.

With ϕ_o and ϕ_1 available we can investigate the differential cross section $I(\theta)$ near $\theta=\pi$. Right at $\theta=\pi$ the differential cross section can be written

$$I(\pi)/a^2 = i(A/E). \tag{45}$$

The function $i(A/E)$ is graphed in Fig. (4). If A is known, an absolute measurement of $I(\pi)$ at a known energy E will give the potential parameter a, but any uncertainty in A will lead to appreciable errors in a. For example, near $A/E=100$ ($R_o \simeq 4.6$) a 10% error in A would change a by 4.9%. The behavior of $I(\theta)$ near $\theta=\pi$ will give (A/E) and thus A, as can be seen from rewriting Eq. (15):

$$\sin\theta(\pi-\theta)^{-1}I(\theta)/I(\pi) = 1-h(A/E)(\pi-\theta)^2+\ldots \tag{46}$$

The behavior of $h(A/E)$ is also shown in Fig. (4). It varies from 1/6 (the hard sphere result) at large A (large R_o) to $-35/(4\pi^2)$ in the limit of $A/E = 1$. This is a somewhat broader range than for the repulsive power potential, but the comments made for the latter potential apply here as well. Either measurements of $I(\theta)/I(\pi)$ must extend to angles considerably smaller than $\theta=\pi/2$ or the measurements

themselves must be very accurate if A is to be determined accurately. Thus, a 1% error in $I(\theta)$ at $\theta=\pi/2$ would give an 8.6% error in A if $A/E \simeq 100$.

The exact differential cross section $I(\theta)$ for the exponential repulsive potential is compared with the series approximation of Eq. (46) in Figure (5). The solid curve shows the angle for each A/E where the exact and approximate (two terms of Eq. (46)) cross sections differ by 5%. The dashed curve shows the angle where the full series expansion in Eq. (10) diverges. As in the case of the repulsive power potential, the two term approximation of $I(\theta)$ works quite well out to $\theta = 90°$ for most values of A/E. The divergence angle falls exponentially, so that for $A/E \gtrsim 1000$ Eq. (46) with a sufficient number of terms would work at all angles. The difficulty would lie in determining the large number of the coefficients ϕ_n.

SHIELDED COULOMB POTENTIAL

The first two coefficients for the shielded Coulomb potential are computed from expressions derived from Eq. (11):

$$\phi_o = (2/a) \int_o^\infty dx \; (x+R_o)^{-3/2}(x+R_o-R_o e^{-x})^{-1/2} \tag{47}$$

$$\phi_1 = a^{-3} \int_o^\infty dx (x+R_o)^{-7/2}(x+R_o+1)^{-2}(x+R_o-R_o e^{-x})^{-1/2} F(x) \tag{48}$$

with

$$F(x) = -5-6(x+R_o) + (x+R_o)^2. \tag{49}$$

Again we have set $R_o=r_o/a$, and it is obtained by solving the equation

$$R_o \exp(R_o) = A/E. \tag{50}$$

In general, ϕ_o and ϕ_1 must be determined numerically, but expansions

for both large R_o and small R_o are easily obtained using the methods of the previous section. For small R_o, e^{-x} is expanded about x=0 and the term $(x+R_o+1)$ is expanded assuming $1>(x+R_o)$. The integrals are then Beta functions, and the results for the expansion are:

$$a\phi_o = 4R_o^{-1}(1+R_o)^{-\frac{1}{2}} \tag{51}$$

$$a^3\phi_1 = -(16/3)R_o^{-3}[1-(3/2)R_o+(27/16)R_o^2]. \tag{52}$$

In the case of large R_o, the term $(x+R_o+1)$ is expanded assuming $1<(x+R_o)$, and the additional expansion

$$(x+R_o-R_oe^{-x})^{-\frac{1}{2}} = (x+R_o)^{-\frac{1}{2}} \sum_{k=o}^{\infty} A_k e^{-kx} \left(\frac{R_o}{x+R_o}\right)^k$$

is used. The resulting integrals are handled similarly to the previous section, and the terms when collected yield

$$a\phi_o = (2/R_o)\sum_{n=o}^{\infty} M_n R_o^{-n} \tag{53}$$

$$a^3\phi_1 = (3R_o^3)^{-1}\sum_{n=o}^{\infty} N_n R_o^{-n}. \tag{54}$$

The first five coefficients M_n and N_n are given in Table IV.

For the intermediate region of R_o where the above series are not useful, we have numerically evaluated ϕ_o and ϕ_1 and fit the values by least squares to polynomials in R_o. These numerical approximations for ϕ_o and ϕ_1 are summarized below:

$0<R_o\leq 0.43$

$$a\phi_o = (3.9997/R_o)\sum_{n=o}^{5} P_n R_o^n \tag{55}$$

$$a^3\phi_1 = (-5.3332/R_o^3)\sum_{n=o}^{4} Q_n R_o^n \tag{56}$$

$0.43\leq R_o\leq 1.60$

$$a\phi_o = (3.9440/R_o)\sum_{n=o}^{4} T_n R_o^n \tag{57}$$

$$a^3\phi_1 = (-5.2370/R_o^3)\sum_{n=o}^{5} U_n R_o^n \tag{58}$$

$1.60\leq R_o\leq 4.63$

$$a\phi_o = (-0.42850/R_o^3)\sum_{n=o}^{4} V_n R_r^n \tag{59}$$

$$a^3\phi_1 = (0.37361/R_o^3)\sum_{n=o}^{5} W_n R_o^{-n} \qquad (60)$$

$4.63 \leq R_o \leq 20.0$

$$a\phi_o = (2.0019/R_o)\sum_{n=o}^{3} Y_n R_o^{-n} \qquad (61)$$

$$a^3\phi_o = (0.33430/R_o^3)\sum_{n=o}^{5} Z_n R_o^{-n} \qquad (62)$$

The various coefficients P_n, Q_n, T_n, U_n, V_n, W_n, Y_n, and Z_n are tabulated in Table V. The accuracy of each series is 1 part in 10^4 for all R_o, except for Eq. (62) which goes through zero near R_o = 5.5. Near R_o = 5.5 the uncertainty is 2×10^{-8} (absolute) or 1×10^{-4} (fractional), whichever is greater.

Using an analysis similar to that for the exponential repulsive potential, we can show that at $\theta=\pi$

$$I(\pi)/a^2 = j(A/E). \qquad (63)$$

Figure (6) graphs j(A/E). Thus, if A/E is known, an absolute measurement of $I(\pi)$ will give a, but any uncertainty in A will lead to errors in a. The ratio of A/E can be determined by the behavior of $I(\theta)$ near $\theta=\pi$ where

$$\sin\theta(\pi-\theta)^{-1}I(\theta)/I(\pi) = 1-H(A/E)(\pi-\theta)^2+ \ldots \qquad (64)$$

The function H(A/E) is also shown in Fig. (6). At large A/E it approaches 1/6 (hard sphere result), whereas at small A/E it levels off at -1/3. This is a much narrower spread than for either of the other two potentials, and the comments made earlier about the necessity for very accurate measurements of $I(\theta)/I(\pi)$ apply even more strongly here. A 1% error in the cross section at $\theta=\pi/2$ would give an 11% error in A if $A/E \simeq 100$.

The approximate differential cross section $I(\theta)$ computed with the two terms of Eq. (64) above is compared with the exact value in

Fig. (7). Once again, we have shown the angle where the two differ by 5%; for angles greater than this the approximate result can be used comfortably. Also shown is the result obtained from Leibfried's[11] study of the convergence of the series in Eq. (10) -- the dashed curve gives the angle where the series diverges. For angles greater than this Eq. (64) with a large number of terms would reproduce $I(\theta)$.

SUMMARY

The behavior of the classical deflection angle θ and the classical differential cross section $I(\theta)$ has been investigated for small impact parameter collisions, where θ is large. The series expansion for θ valid near $\theta=\pi$ has been examined, and expressions for the first two terms of the series have been presented for three simple repulsive potentials. It has been seen that using only these two terms gives accurate values of $I(\theta)$ in the region from $\theta=\pi$ to $\theta\simeq\pi/2$ for most energies. The effect of any experimental error on the derived potential has also been explored. In brief, accurate measurements of $I(\theta)$ in the region $\theta=\pi/2$ to $\theta=\pi$ will yield the repulsive part of the intermolecular potential, but this potential is quite sensitive to experimental uncertainties in $I(\theta)$.

Table I. Coefficients for Expansion of ϕ_0 and ϕ_1 for Large and Small R_0-Exponential Repulsive Potential[a]

n	C_n	G_n	H_n
0	1	1.0000000	1.0000000
1	-3/28	1.3862944	-1.8411169
2	-1/160	-1.3680561	-41.479401
3	-3/4480	3.4067031	116.15040
4	59/215040	-12.699712	-599.30012
5	n.c.[b]	61.608724	3960.7237

[a]See text for description of series.

[b]The integral for this coefficient does not converge.

Table II. Values of $S_n{}^a$

$S_1 = 1.38629436$
$S_2 = 0.68402804$
$S_3 = 0.56778385$
$S_4 = 0.52915486$
$S_5 = 0.51340603$

[a] $S_n = \sum_{k=0}^{\infty} A_k/k^n$, $A_k = \Gamma(2k+1)/[2^k\Gamma(k+1)]^2$.

Table III. Coefficients for Least Squares Fit to ϕ_o and ϕ_1 for Exponential Repulsive Potential[a]

n	D_n	E_n	I_n	J_n	K_n	L_n
0	1.0000 (-0)	1.0000 (-0)	1.00000 (-0)	1.00000 (-0)	1.0000 (-0)	1.0000 (+0)
1	2.3656 (-1)	-1.0688 (-1)	-2.99587 (-1)	9.98720 (-1)	1.3376 (-0)	-2.0026 (+0)
2	-4.947 (-2)	-6.876 (-3)	8.84709 (-2)	-2.79261 (-1)	-7.77 (-1)	-3.7230 (+1)
3	2.007 (-2)	-6.39 (-5)	-1.46877 (-2)	2.69284 (-2)		5.8463 (+1)
4	-5.741 (-3)		1.28299 (-3)	-2.17578 (-3)		-7.107 (+1)
5	7.150 (-4)		-4.5886 (-5)	7.4089 (-5)		

[a]Notation: 2.0(-2) = 2.0×10^{-2}

Table IV. Coefficients for Expansion of[a] ϕ_0 and ϕ_1 for Large R_0-Shielded Coulomb Potential[a]

n	M_n	N_n
0	1.00000000	1.00000000
1	1.3862944	-1.8411169
2	-2.7543504	-39.638284
3	8.2131377	207.63793
4	-35.004643	-1182.7632

[a]See text for description of series.

Table V. Coefficients for Least Squares Fit to ϕ_0 and ϕ_1 for Shielded Coulomb Potential

n	P_n	Q_n	T_n	U_n	V_n	W_n	Y_n	Z_n
0	1.000(-0)	1.0000(-0)	1.0000(-0)	1.00000(-0)	1.0000(-0)	1.00000(+0)	1.0000(+0)	1.00000(+0)
1	-4.924(-1)	-1.4980(-0)	-3.8254(-1)	-1.37590(-0)	-2.6930(-0)	-3.90947(+0)	1.3424(+0)	-2.02694(+0)
2	6.946(-1)	1.6508(-0)	2.4086(-1)	1.18946(-0)	-5.5572(-0)	-1.27030(+1)	-2.0407(+0)	-3.41828(+1)
3	-1.252(-0)	-1.4306(-0)	-9.3195(-2)	-6.79411(-1)	1.2153(-1)	2.63405(+1)	2.084 (+0)	1.21854(+2)
4	1.805(-0)	6.942 (-1)	1.5607(-2)	2.25452(-1)	-7.002 (-3)	-2.39321(+1)		-2.58067(+2)
5	-1.215(-0)			-3.2403 (-2)		8.85366(+0)		2.57289(+2)

References

1. G. E. Ioup and B. S. Thomas, J. Chem. Phys. 50, 5009 (1969).
2. C. Lehmann and G. Leibfried, Z. Physik 172, 465 (1963).
3. F. T. Smith, R. P. Marchi, and K. G. Dedrick, Phys. Rev. 150, 79 (1966).
4. See, for example, E. F. Greene, L. F. Hoffman, M. W. Lee, J. Ross, and C. E. Young, J. Chem. Phys. 50, 3450 (1969).
5. (a) R. M. Felder, J. Chem. Phys. 49, 1438 (1968); (b) R. M. Felder, Brookhaven National Laboratory Report BNL-50102 (1968).
6. E. Everhart, G. Stone, and R. J. Carbone, Phys. Rev. 99, 1287 (1955).
7. M. T. Robinson, Oak Ridge National Laboratory Report ORNL-3493 (1963).
8. D. Burnett, Proc. Cambridge Phil. Soc. 33, 363 (1937).
9. G. Leibfried, Bestrahlungseffekte in Festkorpern (Teubner, Stuttgart, Germany, 1965), p. 37.
10. G. Leibfried and T. Plesser, Z. Physik 187, 411 (1965).
11. Handbook of Mathematical Functions, M. Abramowitz and I. A. Stegun, Eds. (National Bureau of Standards, Washington, D. C., 1964), p. 228.

Figure Captions

Figure 1. The reduced differential cross section at $\theta=\pi$, $i=I(\pi)(E/K)^2/s$, for the repulsive power potential $V=K/r^s$ is shown as the solid curve. The dashed curve gives h, the first coefficient in the expansion of $I(\theta)$ near $\theta=\pi$.

Figure 2. An example of the effect of uncertainty in s when fitting a measured cross section to the potential $V=K/r^s$. For this Figure, E=1 eV and $I(\pi)=0.100\text{Å}^2/\text{sr}$ is assumed to be known, and these data yields the potentials shown if s=6, 7, 8, 9, or 10.

Figure 3. The angle where the approximate (two terms of Eq. (23)) and exact differential cross section $I(\theta)$ differ by 5% is shown as the solid curve for the potential $V=K/r^s$. For angles greater than this the approximate cross section is quite good. For comparison, the dashed curve is the angle where the large-angle series approximation for θ (eq. (10)) diverges.

Figure 4. The reduced differential cross section at $\theta=\pi$, $i=I(\pi)/a^2$, for the exponential repulsive potential $V=A\exp(-r/a)$ is shown as the solid curve. The dashed curve is h, the first coefficient in the expansion of $I(\theta)$ near $\theta=\pi$.

Figure 5. The angle where the approximate (two terms of Eq. (46)) and exact $I(\theta)$ differ by 5% for the potential $V=A\exp(-r/a)$ is the solid curve. The dashed curve is the angle where the large-angle series approximation for θ (eq. (10)) diverges for this potential.

Figure 6. The reduced differential cross section at $\theta=\pi$, $j=I(\pi)/a^2$, for the shielded Coulomb potential $V=A(a/r)\exp(-r/a)$ is shown as the solid curve. The dashed curve is h, the first coefficient in the expansion of $I(\theta)$ near $\theta=\pi$.

Figure 7. The angle where the approximate (two terms of Eq. (64)) and exact $I(\theta)$ differ by 5% for the potential $V=A\,(a/r)\exp(-r/a)$ is the solid curve. The dashed curve is the angle where the large-angle series approximation for θ (eq. (10)) diverges for this potential.

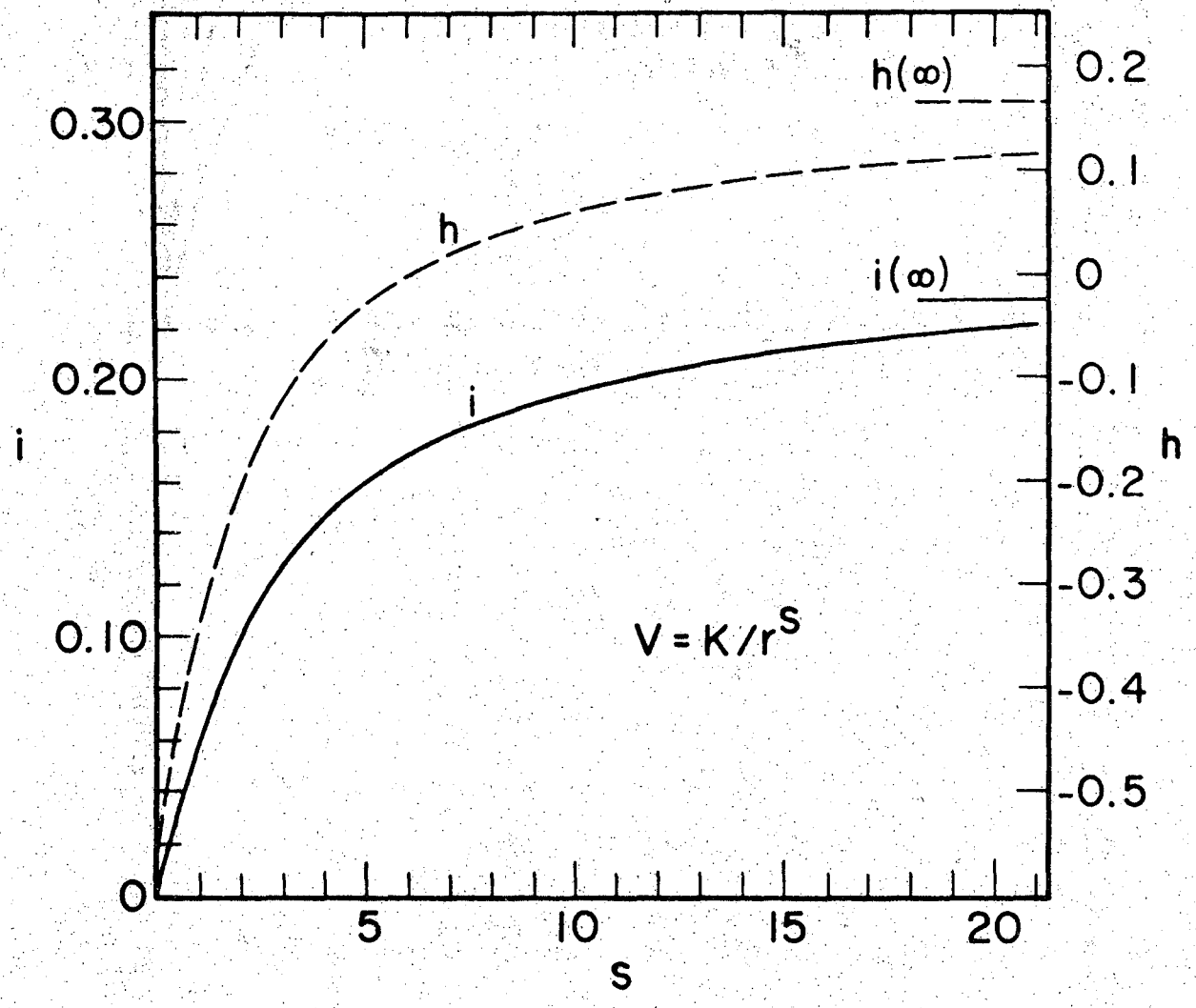

Fig. 1

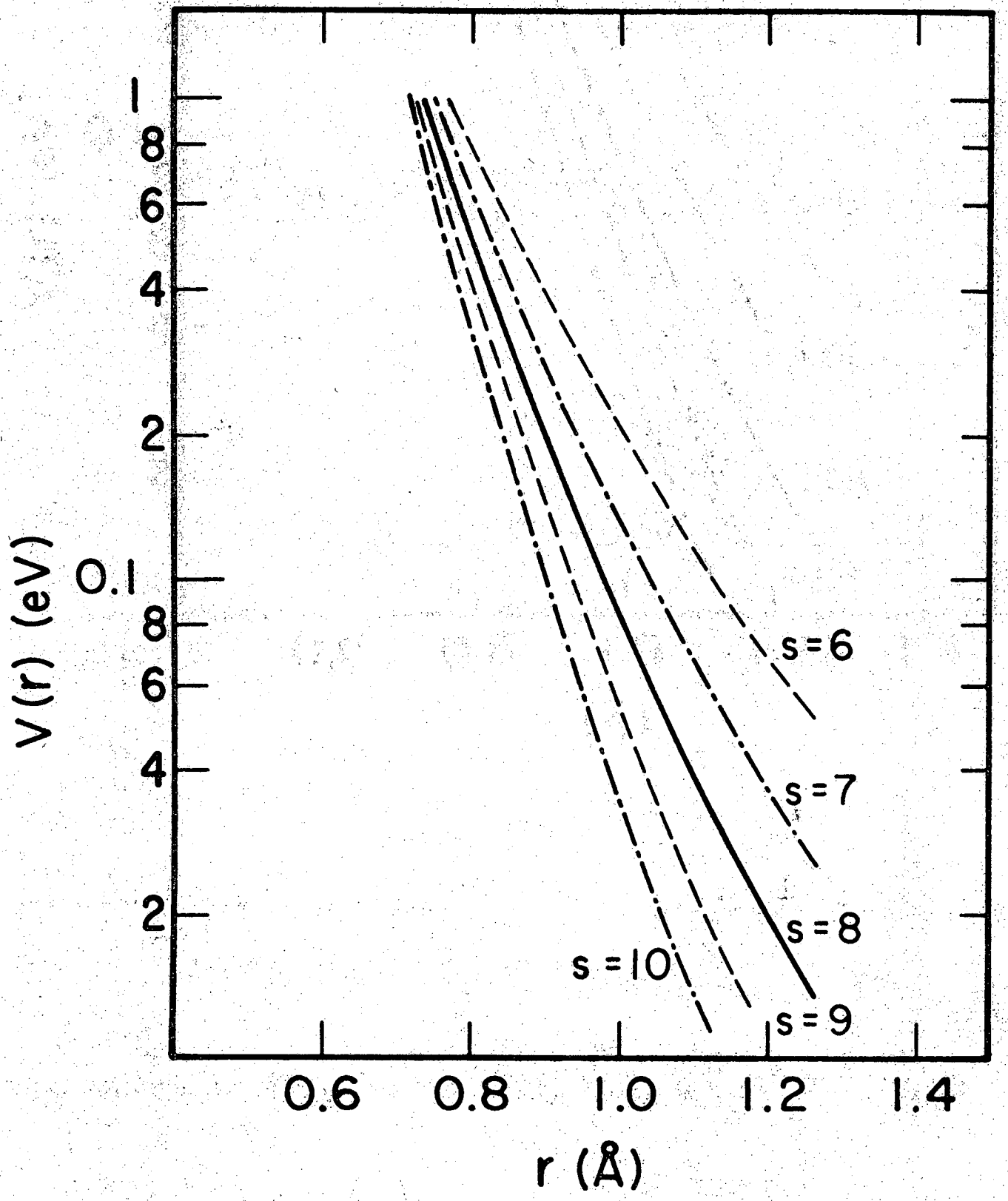

Fig. 2

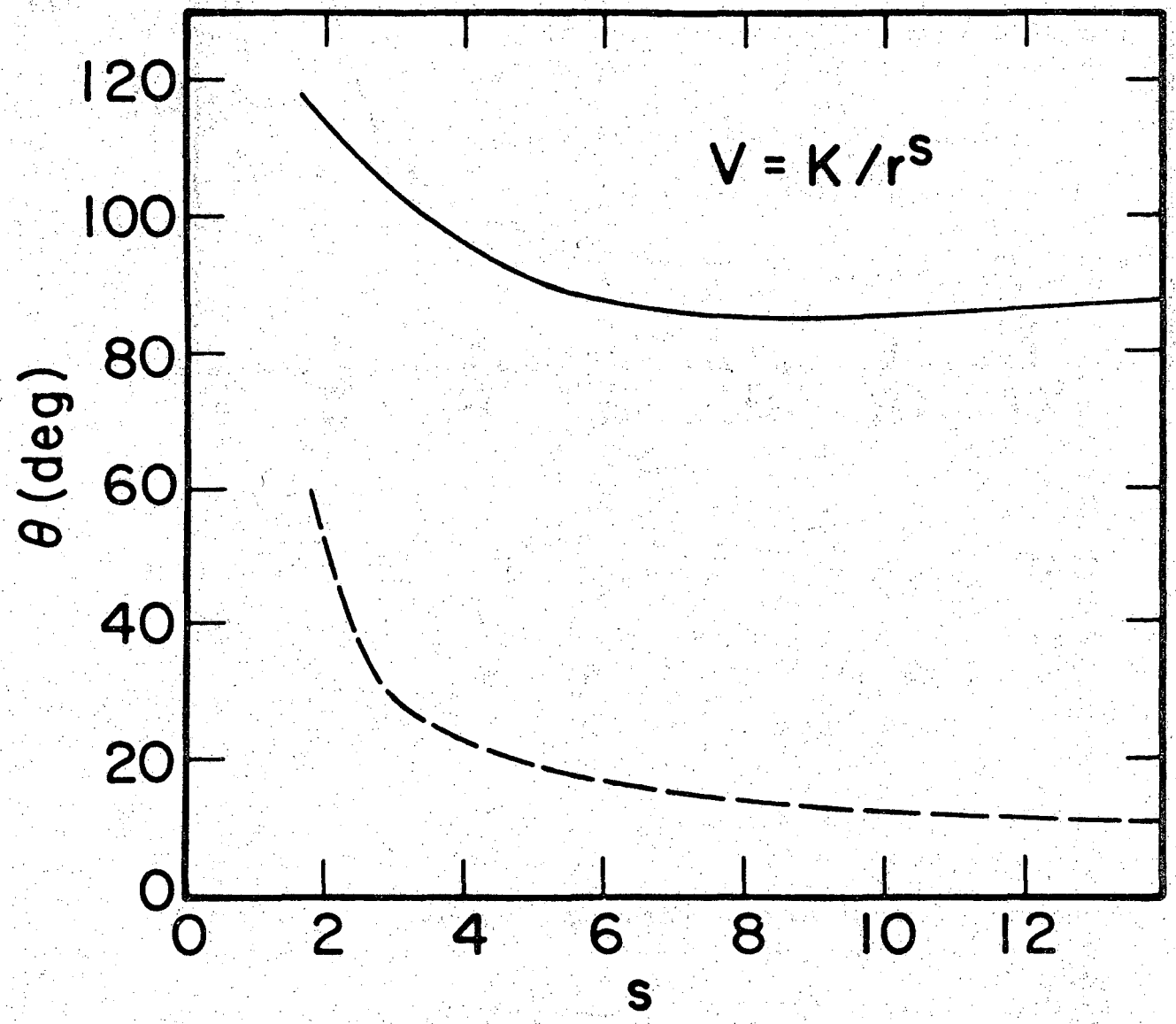

Fig. 3

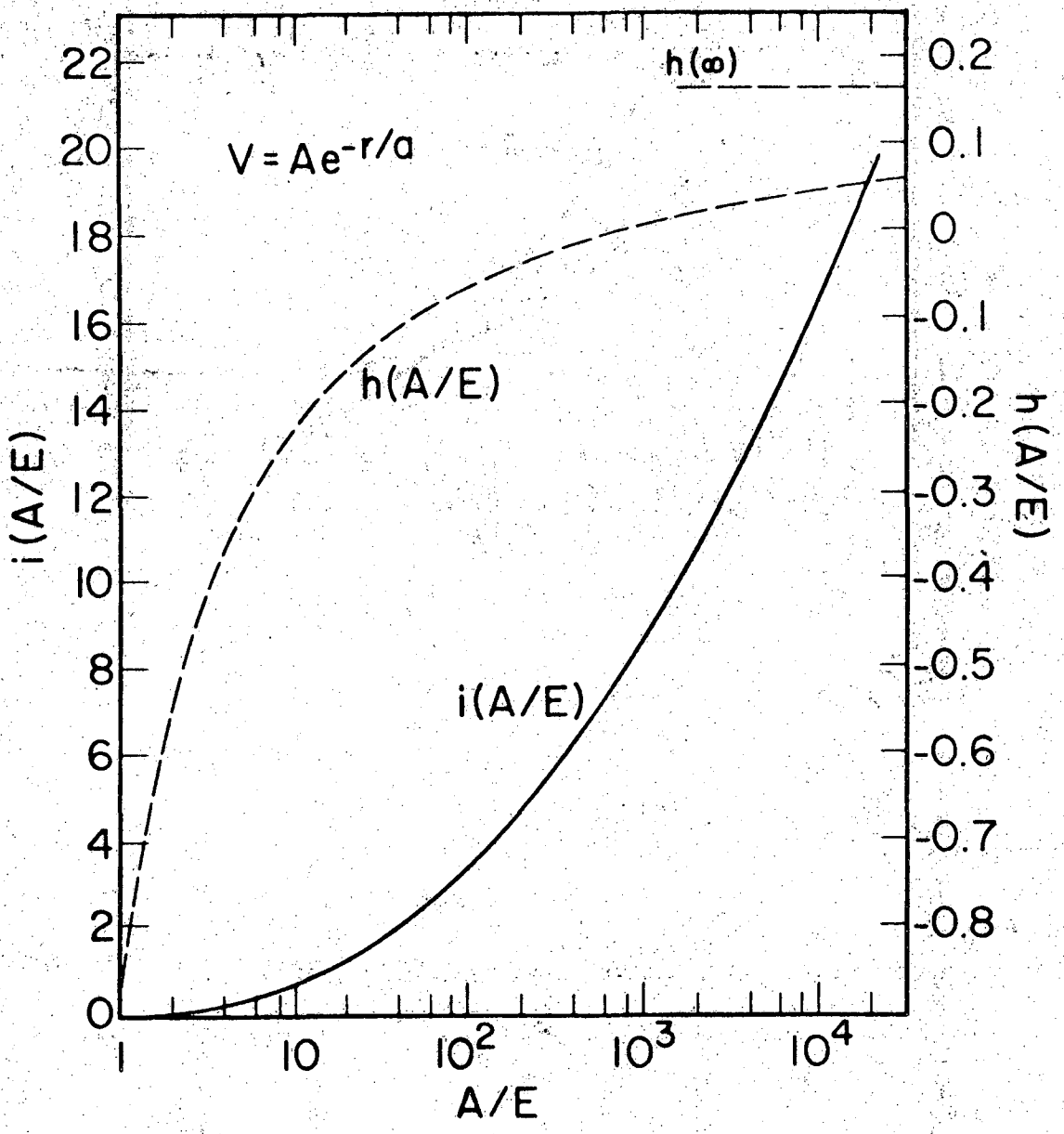
h(∞)
V = Ae^-r/a
h(A/E)
i(A/E)
i (A/E)
h (A/E)
A/E
22
20
18
16
14
12
10
8
6
4
2
0
0.2
0.1
0
-0.1
-0.2
-0.3
-0.4
-0.5
-0.6
-0.7
-0.8
1
10
10^2
10^3
10^4

Fig. 4

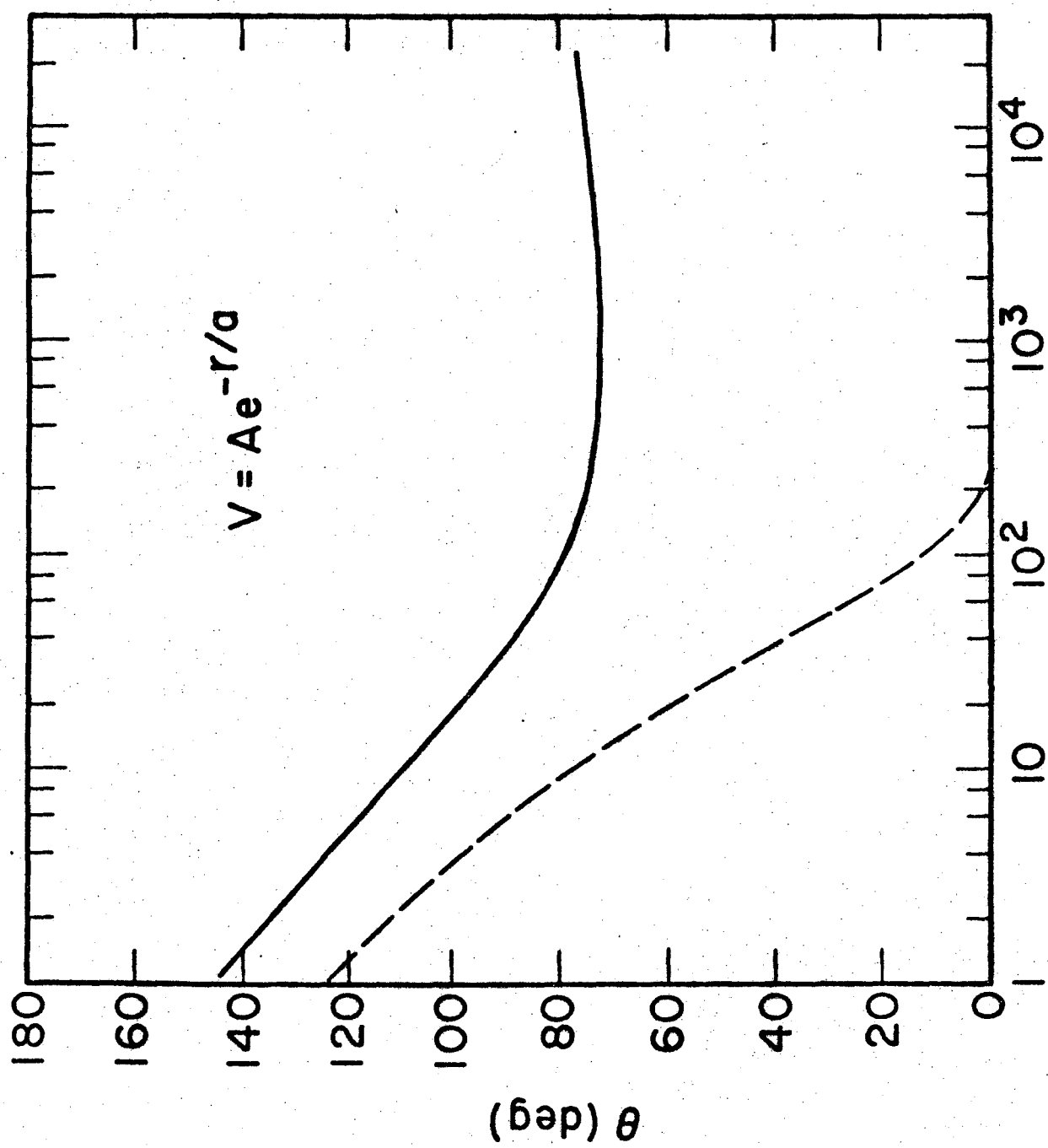

Fig. 5

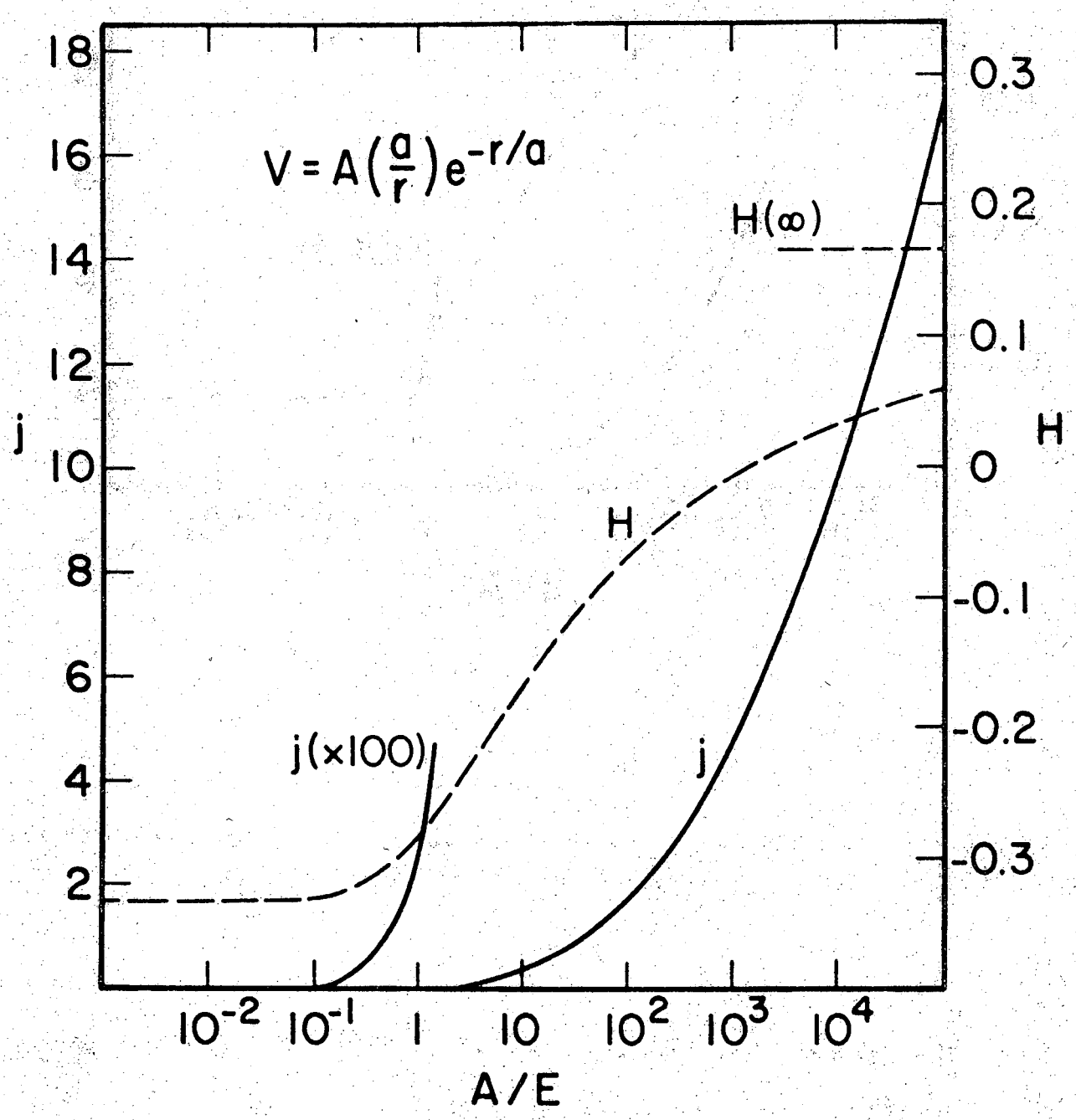
$V = A\left(\frac{a}{r}\right)e^{-r/a}$
H(∞)
H
j(×100)
j
j
H
A/E
18
16
14
12
10
8
6
4
2
0.3
0.2
0.1
0
-0.1
-0.2
-0.3
10^{-2}
10^{-1}
1
10
10^{2}
10^{3}
10^{4}

Fig. 6

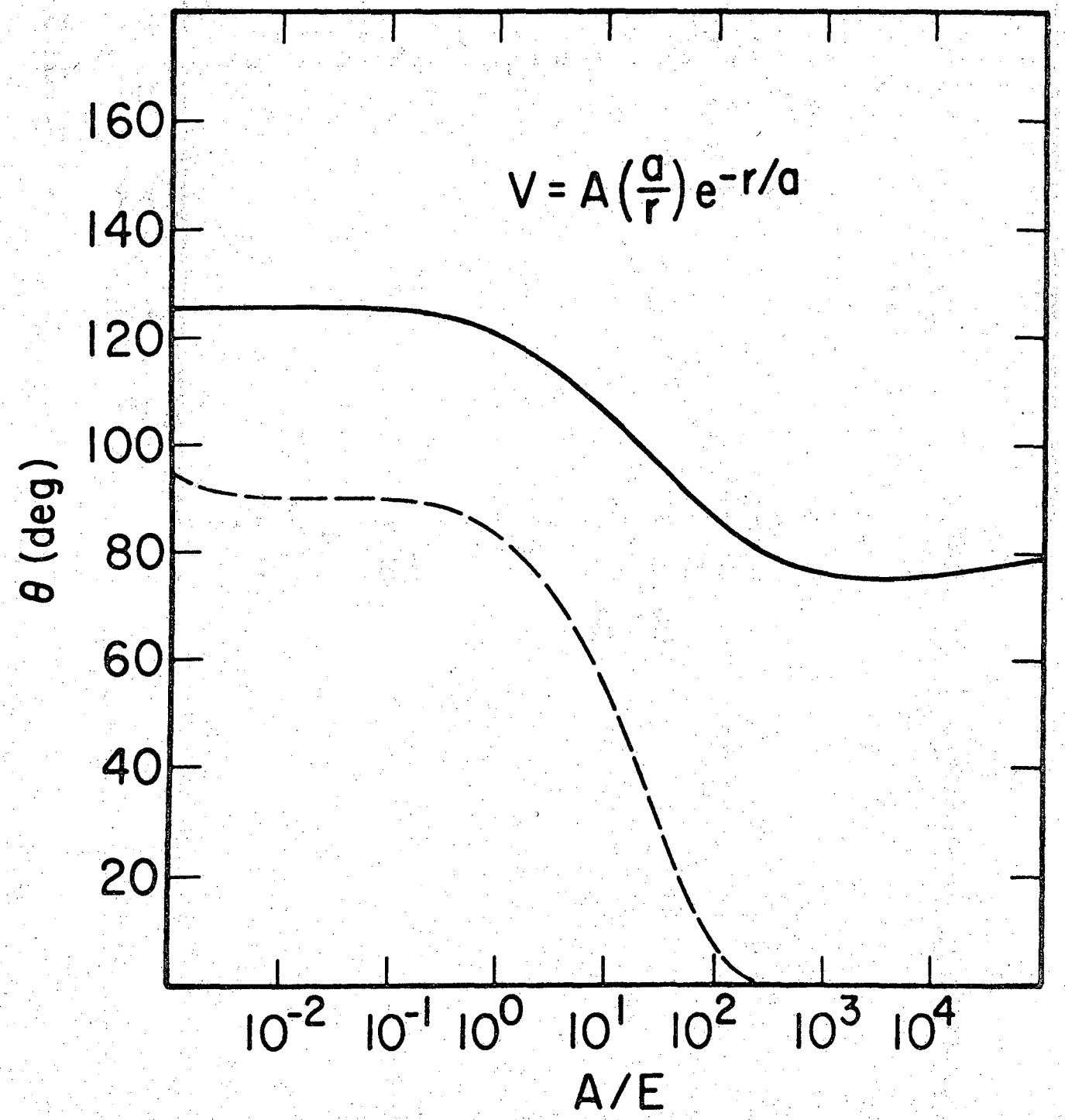
$V = A\left(\frac{a}{r}\right)e^{-r/a}$
160
140
120
100
80
60
40
20
θ (deg)
10^{-2} 10^{-1} 10^{0} 10^{1} 10^{2} 10^{3} 10^{4}
A/E

Fig 7

TECHNICAL INFORMATION DIVISION
LAWRENCE RADIATION LABORATORY
UNIVERSITY OF CALIFORNIA
BERKELEY, CALIFORNIA 94720